APPLIED SCIENCES AND ENGINEERING

Chemical delivery array with millisecond neurotransmitter release

Amanda Jonsson,* Theresia Arbring Sjöström,* Klas Tybrandt, Magnus Berggren,† Daniel T. Simon

Technologies that restore or augment dysfunctional neural signaling represent a promising route to deeper understanding and new therapies for neurological disorders. Because of the chemical specificity and subsecond signaling of the nervous system, these technologies should be able to release specific neurotransmitters at specific locations with millisecond resolution. We have previously demonstrated an organic electronic lateral electrophoresis technology capable of precise delivery of charged compounds, such as neurotransmitters. However, this technology, the organic electronic ion pump, has been limited to a single delivery point, or several simultaneously addressed outlets, with switch-on speeds of seconds. We report on a vertical neurotransmitter delivery device, configured as an array with individually controlled delivery points and a temporal resolution of 50 ms. This is achieved by supplementing lateral electrophoresis with a control electrode and an ion diode at each delivery point to allow addressing and limit leakage. By delivering local pulses of neurotransmitters with spatiotemporal dynamics approaching synaptic function, the high-speed delivery array promises unprecedented access to neural signaling and a path toward biochemically regulated neural prostheses.

INTRODUCTION

The fundamental signaling junctions in the nervous system are the synapses, which relay signals from a presynaptic neuron using fluxes of highly specific neurotransmitters to modulate the membrane potential of the postsynaptic neuron. This chemical signaling occurs at speeds higher than 50 ms between neurotransmitter release and postsynaptic potential (*1*). To date, this high-speed, miniaturized, and highly localized chemical signaling is unattainable with microfluidics or other fluid transport systems (*2*, *3*), and the required on/off dynamics are not possible with methods based on redox-switching of conductive polymers (*4*–*6*). Furthermore, it has been estimated that there are approximately 1 billion synapses per cubic centimeter in the human cortex (*7*) and more than 200,000 neuromuscular junctions in a human bicep (*8*). As with high-speed signaling, these numbers of parallel and independently operating biological connections are beyond our current biotechnological abilities.

To enable deeper understanding of signaling and next-generation therapies capable of approaching the spatiotemporal resolution and chemical specificity of neurons and their synaptic connections, we have developed the organic electronic ion pump (OEIP). The OEIP electrophoretically transports ions (for example, Na^+, Ca^{2+}, and charged neurotransmitters) through a hydrated polyelectrolyte film, functioning as a cation (or an anion) exchange membrane. The selectivity of this membrane for only cation (or anion) transport provides OEIP technology with the ability to administer precise amounts of signaling compounds, with rapid on/off switching, and without requiring liquid flow. OEIPs have not only been used in vitro to trigger cell signaling (*9*, *10*) and to control epileptiform activity in brain slices (*11*) but also in vivo to affect sensory function (*12*) and as a therapy for pain in conscious animals (*13*).

However, these OEIP-based devices rely on lateral electrophoretic transport through the ion exchange membrane. With such an architecture, OEIPs can achieve speed records of ~200 ms between switching on the voltage and delivering ions to the target region, but this requires a complicated prefilling system (*10*) and is still far too slow for synaptic dynamics. Decreasing this turn-on time would require very short transport channels, resulting in large concentration gradients, which could lead to significant leakage, as well as encapsulation and liquid isolation that would be difficult to achieve at such small scales. Furthermore, achieving individual addressing of several release sites with existing OEIP technology would be difficult, as the required electrode and electrolyte for each release site would be difficult to integrate.

To achieve high-speed delivery, we have developed a new paradigm for OEIP and other such "iontronic" devices (*14*, *15*). We significantly reduced the distance ions travel before release to a few micrometers by building devices where we can control transport (electric fields) not only laterally but also vertically through the thin films (Fig. 1). Augmenting the OEIP channel with this additional functionality in the form of a control electrode under each outlet also provides independent addressability of individual outlets, as described below. The new architecture thus provides an addressable refillable ion delivery array (ARIDA). A single "pixel" device consists of a cation-conducting (and electronically insulating) channel and a cation-conducting (and electronically conducting) control electrode covered by an additional polycation layer, placed in the center of a "standard" OEIP. The full multioutlet ARIDA consists of several of these channels in parallel (Fig. 1F). As with the OEIP, the source electrolyte, containing the molecules to be delivered, is placed at one end of the channel, and a waste electrolyte/electrode (what would have been the target system in previous OEIPs) is placed at the other end. Cations are transported from source to waste in the plane of the substrate, but when they reach the ARIDA outlets, they can be diverted perpendicularly into a target electrolyte placed between the other electrolytes, depending on the voltage applied to the control electrode (Fig. 1B).

RESULTS

The main cation-permselective cation-conducting channel comprises poly(styrene sulfonate-*co*-maleic acid) (PSSA-*co*-MA) cross-linked with poly(ethylene glycol) (PEG). The control electrode, consisting of poly(3,4-ethylenedioxythiophene):poly(styrene sulfonate) (PEDOT:PSS), is simultaneously cation-permselective (see the Supplementary

Laboratory of Organic Electronics, Department of Science and Technology, Linköping University, 601 74 Norrköping, Sweden.
*These authors contributed equally to this work.
†Corresponding author. Email: magnus.berggren@liu.se

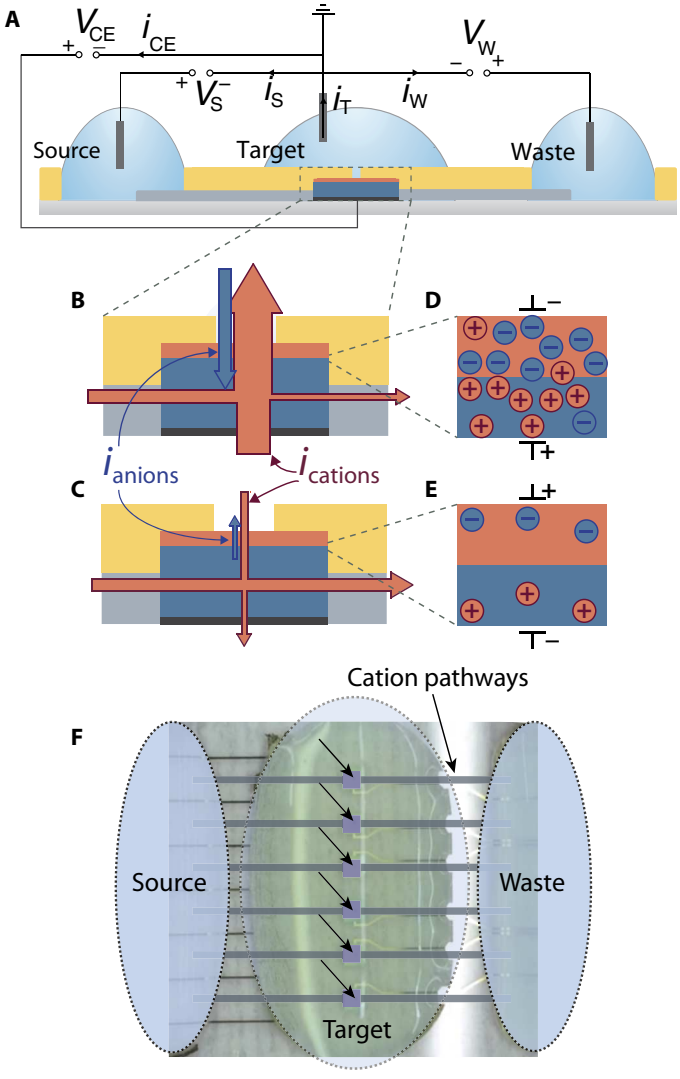

Fig. 1. Architecture of device and ionic currents. (**A**) Side view of a device showing the three electrolytes (source, target, and waste) with their potentials set by the electrodes to V_S, $V_T = 0$, and V_W, respectively. The V_{CE} is set to positive values to switch delivery on and to negative values to switch delivery off, with respect to the grounded V_T. The dark gray material illustrates the cation-selective polyanion, which is the pathway for cations from the source to the waste; the PEDOT:PSS control electrode is depicted in blue, and the anion-selective polycation is depicted in red. In general, a positively charged material is depicted in red, and a negatively charged material is depicted in gray or blue. The encapsulation material is shown in yellow. (**B**) Cationic and anionic currents when delivery is on. (**C**) Ionic currents when delivery is off. (**D**) Ions accumulate at the internal interface of the BM when delivery is on and when the BM diode is in forward bias. (**E**) Reverse-bias of the BM diode leads to ion depletion in the BM interface, which limits the currents. (**F**) Top view of array comprising six of the structures in (A) in parallel. Arrows point to six delivery points in a common target electrolyte.

Materials) (*16*, *17*) and electronically conducting (*18*). Finally, the polycation capping the control electrode at each outlet is poly(vinylbenzyl chloride) quaternized by *N*-benzyldimethylamine and cross-linked with 1,4-diazabicyclo[2.2.2]octane (qPVBC). Together, the cation-permselective PEDOT:PSS and the anion-permselective qPVBC form a bipolar membrane (BM) with ion current rectification properties (*19*, *20*), yielding a high cationic delivery current to the target electrolyte when the control electrode is positive (Fig. 1B), but a low current (in the opposite direction) when the control electrode is negative, with respect to the target potential (V_T) (Fig. 1C). Positive control electrode potential (V_{CE}) leads to an accumulation of anions and cations at the qPVBC/PEDOT:PSS interface, resulting in Donnan failure (*21*, *22*) of both materials; that is, the materials lose their permselectivity, anions migrate into the cation-permselective PEDOT:PSS, and cations migrate through the anion-permselective qPVBC to the target (Fig. 1D). Negative V_{CE} instead depletes the interface of ions, limiting the current (Fig. 1E). The BM at each ARIDA outlet thus acts as an individually addressable switch controlling whether ion transport is solely from source to waste (lateral) or directed into the target system (vertical).

To verify whether cations could be transported from the source to the waste without leakage to the target, we placed HCl(aq) in the source, added a pH indicator to the target and waste electrolytes, and applied the potentials [V_{CE}, V_S (source potential), and V_W (waste potential) = −0.2 V, +1.5 V, and −1.9 V, respectively]. After a few minutes, a color change was observed in the waste solution, indicating the delivery of protons, but no color change was observed in the target, indicating negligible leakage. When switching V_{CE} to +0.7 V to activate vertical delivery into the target, a color change was observed in the target within seconds (Fig. 2B) (see the Supplementary Materials for details). This delivery could be switched on and off several times, with similar color change observed for each pulse (fig. S1 and movie S1).

With the basic functionality demonstrated, we proceeded to assess the enhanced dynamics of the ARIDA structure, transporting the neurotransmitter acetylcholine (Fig. 2A). To estimate the switch-on time of acetylcholine release, we applied positive V_{CE} pulses of different durations and analyzed the resulting concentration of the neurotransmitter in the target solution (Fig. 2D). V_{CE} was applied for 1000 s as a square wave between +0.7 and −0.4 V with a 20% duty cycle; that is, delivery was on for "pulse length" τ and off for 4τ, with τ varying from 2 to 1000 ms. V_S and V_W were adjusted during the experiment to keep the target/delivery current, i_T, negative ("down," out of the target system), around −20 nA between pulses. With delivery kept off in this manner (V_{CE} = −0.4 V) for 1000 s, 130 pmol of acetylcholine was detected in the target solution, indicating that the BM structure did not completely prevent diffusive leakage (see the Supplementary Materials and fig. S2). However, once delivery was activated with τ reaching 50 to 100 ms, a clear increase in the acetylcholine concentration could be observed. The on/off is defined as the amount of acetylcholine released per unit time with delivery on divided by the amount released per unit time with delivery off. For τ = 100 ms, the on/off was 8.2, and for τ = 1 s, the on/off was 21 (see the Supplementary Materials). By fitting a simple model to the data (fig. S3), we estimate that the threshold before delivery starts—that is, the time between voltage-on and ion delivery, or the maximum delivery response—was 50 ms. This delay may be related to initial spikes in i_T, followed by a leveling out of the current (Fig. 2C and fig. S4), suggesting mixed capacitive and resistive currents.

To verify ion delivery from multiple, individually addressed outlets, we fabricated devices with six outlets (Fig. 1F). HCl(aq) (0.1 M) was used as source electrolyte, and a pH indicator was added to the 0.1 M KCl target and waste solutions. Proton delivery could be observed as a color shift from green to red. When delivery was first turned on, V_{CE} was kept at −0.4 V at all outlets (all outlets "off"). Red clouds appeared in the waste, indicating that the channels had been filled with protons, and no color change was observed at any outlet in the target electrolyte. The outlets were then individually addressed in sequence by shifting

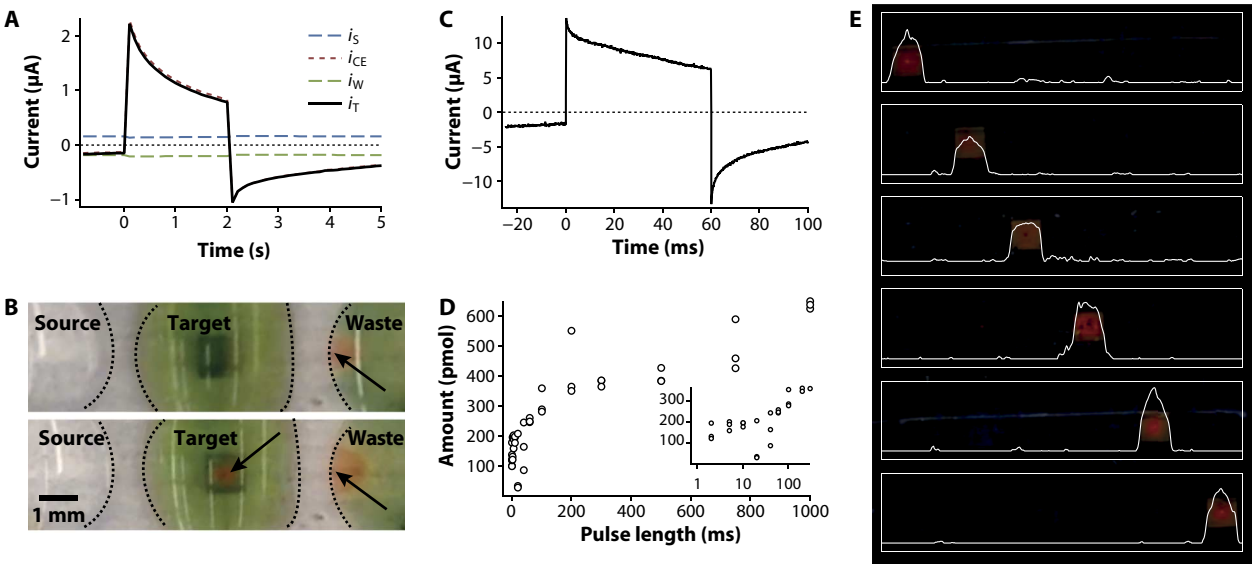

Fig. 2. Characterization of ion delivery. (**A**) Typical currents when delivering acetylcholine during a 2-s-long pulse [V_{CE}, V_S, and V_W = −0.2 V (<0 and >2 s)/+0.7 V (0 to 2 s), +7 V, and −7 V]. (**B**) Protons were loaded into the source, and the pH indicator was added to the target and the waste. A potential between source and waste was applied. With the BM diode reverse-biased (V_{CE} = −0.4 V with respect to V_T), no color change indicating proton delivery was observed in the target (top). With the BM diode in forward bias (V_{CE} = +0.7 V), a red cloud appeared at the delivery point (arrow, bottom). (**C**) Delivery current versus time for 60-ms-long delivery pulses of acetylcholine (V_{CE} = −0.2 V/+0.7 V). (**D**) Measured amount of acetylcholine in the target after 1000 s of delivery with pulse lengths varying from 2 to 1000 ms, using a 20% duty cycle. The inset is a close-up of pulse lengths up to 200 ms, with logarithmic time scale. (**E**) Protons could be delivered separately from all six pixels in the array (Figs. 1F and 3E). Images show the color-adjusted pH response (profile shown as white line). Each row is a separate image, where delivery was on in pixel 1 on row 1, pixel 2 on row 2, etc. Delivery is only apparent in the addressed pixels, which suggests low leakage from the reverse-biased pixels. The original color image can be seen in fig. S5.

V_{CE} of the corresponding site from −0.4 to +0.7 V relative to V_T, and color shifts were observed at the addressed outlets (Fig. 2E and fig. S5). The outlets in the 2D array were 100 μm × 100 μm and separated by 2 mm to show that each pixel could be individually addressed. Arrays with 200-μm spacing between 20 μm × 20 μm delivery points were also fabricated and performed similarly (fig. S6).

Lateral migration of cations from the source, through the control electrode, and out to the waste electrolyte is achieved by applying a positive V_S and negative V_W while keeping the V_{CE} slightly negative with respect to the V_T (V_T = 0), to reverse-bias the BM diode and prevent delivery to the target. V_{CE} affects the potential of cations in the PEDOT:PSS control electrode, as long as the PEDOT:PSS is not completely reduced. As the PEDOT in the control electrode is reduced (becomes more neutral), i_{CE} approaches zero, and the PEDOT:PSS potential is determined by V_S and V_W, rather than by V_{CE}. While filling the channel with cations, we balance the currents such that the PEDOT:PSS pixel is reduced ($i_{CE} \leq 0$), and the BM diode is reverse-biased, that is, the delivery current is negative. To switch on delivery, V_{CE} is made positive with respect to V_T, setting the diode in forward bias and changing the direction of the electric field between the control electrode and the outlet such that cations migrate to the target. The potential experienced by a cation migrating from source to target is thus highly affected by the polarity of V_{CE} (Fig. 3, A to C). As V_{CE} is changed from negative to positive, neutral PEDOT in the control electrode becomes oxidized (increasingly positively charged). As $PEDOT^+$ compensates for the negative PSS^-, mobile cations present in the control electrode are released and delivered to the target. Conversely, when V_{CE} is made negative, the positive charge of PEDOT is decreased, and cations enter the polymer to compensate for the fixed PSS^- and keep the material charge neutral. In this way, the negative V_{CE} used to prevent delivery also stores cations in the PEDOT:PSS control electrode near the delivery site.

With the geometry and materials presented here, delivery can be off for long times, but it cannot be on for longer than a few seconds, because keeping V_{CE} positive risks overoxidizing and thus destroying the PEDOT. In addition, anions may fill the PEDOT:PSS bulk and move toward the source, which could lead to swelling and the eventual collapse of the device. The device is instead constructed to deliver ions in short pulses (a few milliseconds to a few seconds), separated by enough time to reset the device, that is, to empty the anion exchange membrane of cations and the PEDOT:PSS of anions, thus depleting the BM interface and filling the PEDOT:PSS with new cations from the source.

When a delivery pulse is initiated, cations are repelled from the PEDOT:PSS in a fashion analogous to the discharge of a capacitor. To capture the dynamic behavior of switching delivery on and off, we modeled our device as an equivalent electrical circuit (Fig. 4). The equivalent circuit model explains how an ionic current can flow from the source electrolyte and "charge" the upper plate of the control electrode capacitor (C_{CE}) with cations, while PEDOT is reduced. When the capacitor is discharged, cations are released to the target and waste. The model can qualitatively describe the dynamic current-voltage behavior when switching delivery on and off (fig. S7) and can be useful for future optimization and integration into larger bioelectronic systems.

DISCUSSION

We have demonstrated an electrically controlled chemical delivery circuit, where charged compounds can be released independently from several delivery points within tens of milliseconds. The introduction of control electrodes under each delivery point, enabling the establishment of vertical potential gradients through the device's thin films, is

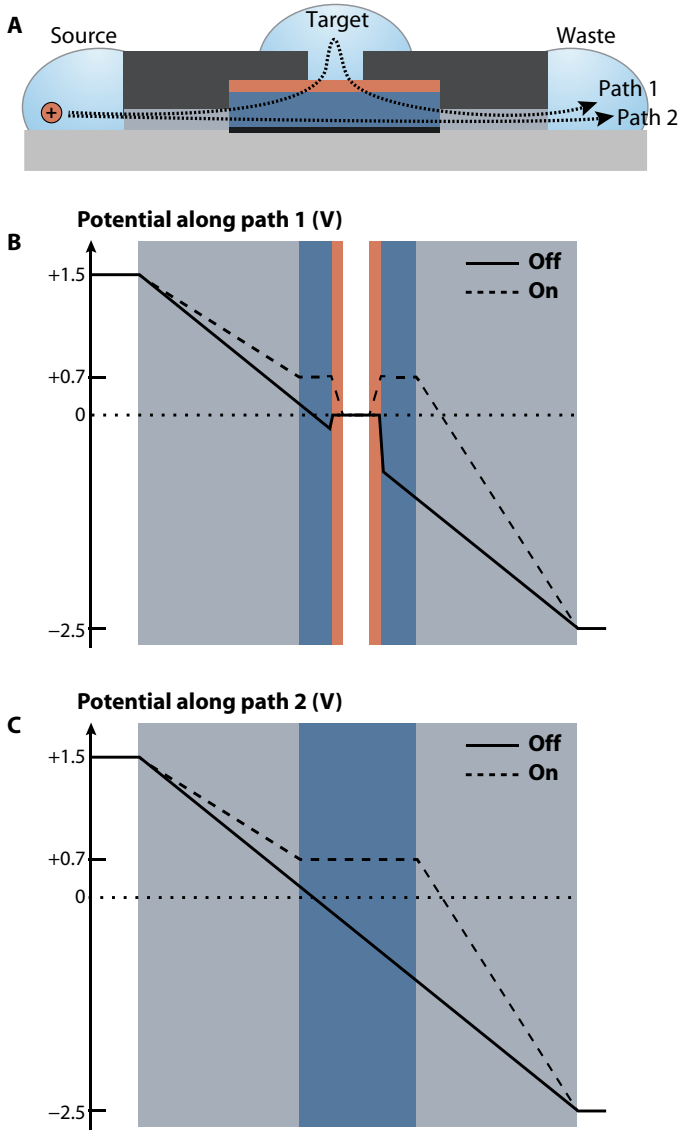

Fig. 3. Transport and switching mechanism. (**A**) Schematic side view of the device showing two hypothetical paths for cations. The polyanionic channel is depicted in dark gray, the PEDOT:PSS electrode is depicted in blue, and the polycationic layer is depicted in red. (**B**) Potential profile experienced by a cation following path 1 and (**C**) potential profile experienced by a cation following path 2. Both (B) and (C) illustrate the potential when the PEDOT:PSS control electrode has just been switched on (dashed line) and when delivery is statically off (solid line). The potential in the PEDOT:PSS is raised above zero by the control electrode when delivery is on (V_{CE} = +0.7 V) but lower when delivery is off, which explains why delivery should only occur from the positively biased control electrodes.

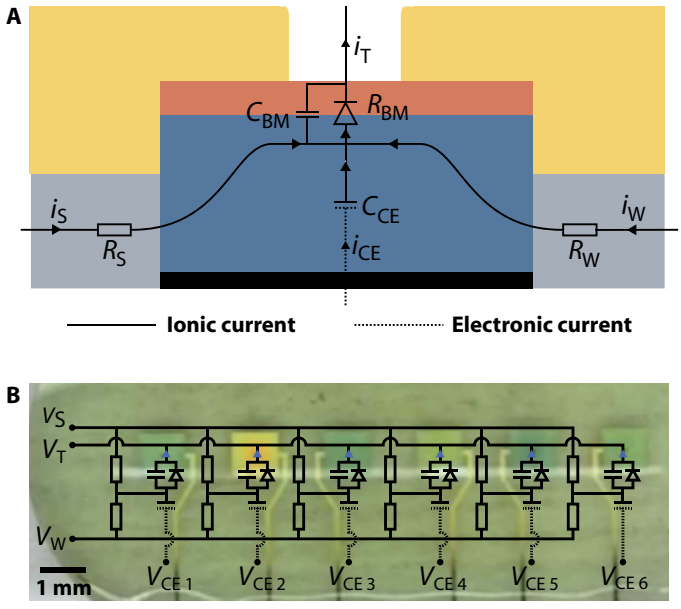

Fig. 4. Simplified equivalent circuit. (**A**) Equivalent circuit describing the dynamic ion discharge from the PEDOT:PSS when delivery is switched on. BM diode is modeled as a capacitor and a diode in parallel, C_{BM} and R_{BM}, whereas the PEDOT:PSS is modeled as a capacitor. (**B**) Array circuit overlaid over an image of the actual array. Blue arrowheads indicate the delivery currents from each delivery point. In the underlying image, only $V_{CE\,2}$ has been addressed to deliver protons.

the main development compared to our previous work. By separating each delivery point and its control electrode with a BM diode, a high resistance is achieved when the diode is reverse-biased. The diode thus suppresses diffusive leakage while limiting the reverse current, thereby avoiding depleting the outlet region of ions and disrupting the local biological environment (*23*). In forward bias, the diode has a much lower resistance; when delivery is switched on, high delivery currents can be achieved.

Although reverse-biasing the diodes prevented diffusive leakage, we still observed diffusion of 0.1 pmol·s^{-1}. We believe that the electric field across the BM diode was not large enough to completely prevent diffusional leakage. At higher field strengths, we observed electric field–enhanced water dissociation, and more negative potentials risk side reactions such as oxygen reduction at the PEDOT electrode. We thus chose not to lower V_{CE} below −0.4 V versus Ag/AgCl. We believe that by optimizing the geometry and materials, we could better prevent passive leakage. Likewise, in the above experiments, 0.1 pmol of acetylcholine was delivered within 100 ms, but this amount can be optimized by modified geometry (outlet size and thickness of different layers) and materials (porosity and charge density) (see the Supplementary Materials).

Another issue is that the polycation of the BM diode hinders the transport of large cations, which limits the use of the device to smaller compounds (for example, neurotransmitters and amino acids). To enable the delivery of larger ions, we are currently working on new polyelectrolytes and diodes using geometric restrictions (high aspect ratio outlets) in place of the polycation (*24*).

The devices were made by photolithographic patterning of metal contacts and polymers, allowing for scaling up to large area arrays or matrices with hundreds of delivery points. With this technology, time-varying concentration gradients could be generated across two-dimensional (2D) areas, such as a microscopy slide or a petri dish. These 2D high-speed "chemical displays" would enable unprecedented study of neural signaling in cell cultures or tissue slices and begin the path toward highly parallel bioelectronic chemical interaction with functional neural networks. Finally, the devices presented above were fabrication on planar glass substrates for use in vitro, but the technology could be adapted for implantable application. With high-speed neural signaling in vivo, ARIDA technology could provide new tools for the most demanding neuromodulation applications, including epilepsy and neural prostheses.

MATERIALS AND METHODS

Device fabrication

Glass discs (4 inches in diameter; Specialty Glass Products) were cleaned using soap, acetone, isopropanol, and water. Photoresist Shipley S1813 G2 was spin-cast on the substrates, exposed using a MA6/BA6 Süss Mask and Bond Aligner, and developed in Microposit MF319 to obtain the pattern for the gold electrodes and contacts. Titanium and gold (approximately 20 and 100 nm, respectively) were evaporated (Balzers BA 510), and the photoresist along with excess metal was lifted off using acetone.

The glass discs with the patterned gold were then treated with ultravioltet ozone (Jelight, 144AX-220) for 60 min. The adhesion promoter 3-glycidoxypropyltrimethoxysilane (GOPS; 1 ml) was added to ethanol (47.5 ml), water (2.5 ml), and acetic acid (50 µl) and mixed for 15 min, and then the glass discs were soaked in the GOPS solution for 1 min. The discs were then quickly rinsed in ethanol, dried, and baked for at least 15 min at 110°C. PSSA-*co*-MA (4 wt % in a water/1-propanol mixture, 1:2.6) was mixed with PEG (1.5 wt %; molecular weight, 400) for cross-linking and then deposited by spin-coating at 1500 rpm to obtain a thickness of approximately 250 nm. The substrates were then baked at 110°C for at least 1 hour. A thin layer of poly(methyl methacrylate) (PMMA; Sigma-Aldrich; average molecular weight, 12,000, 4 mg/ml in diethyl carbonate) was deposited on top of the PSSA-*co*-MA film for improved adhesion of the photoresist. The photoresist Shipley S1813 G2 was then deposited, exposed, and developed in Microposit MF319. Reactive ion etching [O_2, 100 standard cubic centimeter per minute (SCCM); CF_4, 200 SCCM, 150 W, 90 s] was used to obtain the patterns of PSSA-*co*-MA. The remaining photoresist and PMMA were removed using acetone.

Next, photoresist Shipley S1813 G2 was deposited and patterned to obtain protection for the patterned PSSA-*co*-MA and holes for the PEDOT:PSS. The patterned photoresist was treated with oxygen plasma to improve the wetting of the PEDOT:PSS solution. Twenty milliliters of PEDOT:PSS (Clevios PH 1000) was mixed with 1 ml of ethylene glycol, 50 µl of dodecylbenzene sulfonic acid, and 1 wt % GOPS. Water was first spin-cast on the substrates, and then three layers of the PEDOT:PSS solution were deposited at 1500 rpm (with 30-s baking at 110°C on a hot plate between the layers), resulting in approximately 1-µm-thick films.

A solution of qPVBC was prepared. Dimethylbenzylamine (76 µl) was mixed with poly(vinylbenzyl chloride) (200 µl) in tetrahydrofuran (200 mg/ml) and heated in a water bath at 50°C for 1 hour. The precipitate was washed in acetone and dissolved in 1 ml of water and 1 ml of 1-propanol, and 7 µl of the cross-linker diazabicyclo[2.2.2]octane (5.5 M) was added. The qPVBC was then spin-coated (4000 rpm), and the substrates were baked for at least 1 hour at 110°C. A layer of PMMA (Sigma-Aldrich; average molecular weight, 12,000, 40 mg/ml in diethyl carbonate) was deposited and baked (90 s at 110°C), and another layer of photoresist Shipley S1818 G2 was spin-cast and patterned to cover the PEDOT:PSS delivery electrodes with qPVBC on top. The devices were dry-etched, and excess photoresist and PMMA were removed in acetone to obtain the PEDOT:PSS and qPVBC delivery electrodes.

Finally, the devices were encapsulated with SU-8 3010 (MicroChem). The SU-8 was spin-coated at 3000 rpm, soft-baked for 10 min, including a ramping from 65° to 95°C, exposed, postexposure-baked for 1 min at 95°C, and developed in mr-Dev 600, resulting in approximately 10-µm-thick films. The SU-8 pattern defined small delivery outlets on top of the control electrodes as well as hydrophobic confinements for the three electrolytes: source, waste, and target. A final bake was carried out at 110°C for at least 5 min before painting Ag/AgCl electrodes in the confinements for the source, waste, and target electrolytes.

Current-voltage characterization

The devices were soaked in deionized water at least 30 min before the measurements. KCl(aq) (0.1 M) was used for target and waste electrolytes, unless otherwise stated. The pH indicator (Fluka 36828, Sigma-Aldrich) was added to the KCl. HCl(aq) (0.1 M) was used as source electrolyte for the proton experiments. Keithley 2602A and Keithley 2612 SourceMeters and custom LabVIEW code were used to characterize the devices.

Verification of individual addressability (Fig. 2E)

The array was configured with the pH indicator in the target solution, as for the current-voltage characterization. An image was taken a few seconds before and a few seconds after delivery was initiated, and the first image was subtracted from the second. When each pixel was addressed, the color change in the pH indicator indicated individual activation of the pixel. The red channel was separated from the composite image, and a color profile tool was used to extract the profile of the red signal to detect any leakage from adjacent pixels.

Assessment of switch-on time of delivery

Acetylcholine chloride (aq) (0.1 M) was placed on the source reservoir, and 0.1 M KCl(aq) solutions were placed on the target and waste reservoirs. A waveform generator (Agilent 33250A) was configured to pulse a square wave voltage to the delivery electrode versus the target electrode, which was grounded (+0.7 V/−0.4 V, 20% duty cycle). A Keithley 2612 SourceMeter was used to apply voltages to the source electrode and the waste electrode with respect to the grounded target electrode. An oscilloscope (Agilent Infiniium 54830) was used to measure the target current by measuring the voltage across a resistor (10× to 100× lower resistance than the respective resistances of the device) connected in series with the target. Different pulse lengths were used (2 to 1000 ms), but the duty cycle was always set at 20%. The target solution was collected every 1000 s, and 20 µl of deionized water was placed on the target reservoir and added to the collected target solution to make sure that most of the acetylcholine was collected. The concentration of acetylcholine in the collected samples was then measured using an Amplex Red Acetylcholine/Acetylcholinesterase Assay Kit (A12217, Molecular Probes) and a plate reader (Synergy H1, BioTek).

SUPPLEMENTARY MATERIALS

Supplementary material for this article is available at http://advances.sciencemag.org/cgi/content/full/2/11/e1601340/DC1

Permselectivity of PEDOT:PSS
Prevention of passive leakage
Simple model of delivery
Equivalent circuit modeling
fig. S1. Delivery of H^+ from a 1-mm × 1-mm large control electrode, with a 20-µm hole.
fig. S2. Suppression of diffusive leakage of acetylcholine by reverse-biasing the control electrode.
fig. S3. Fit of delivery data to determine maximum dynamics (same data as Fig. 2D).
fig. S4. Delivery currents for various pulse length τ.
fig. S5. Original images showing how one delivery site in each image has been addressed.
fig. S6. Image of an array with biologically relevant pixel spacing (200-µm spacing between pixels).
fig. S7. Simulated 5-s delivery pulses using simple circuit model.
Movie S1
Reference (*25*)

REFERENCES AND NOTES

1. S. A. Siegelbaum, E. R. Kandel, R. Yuste, in *Principles of Neuroscience*, E. R. Kandel, J. H. Schwartz, T. M. Jessell, S. A. Siegelbaum, A. J. Hudspeth, Eds. (McGraw-Hill Professional, ed. 5, 2013).
2. G. M. Whitesides, The origins and the future of microfluidics. *Nature* **442**, 368–373 (2006).
3. I. R. Minev, P. Musienko, A. Hirsch, Q. Barraud, N. Wenger, E. M. Moraud, J. Gandar, M. Capogrosso, T. Milekovic, L. Asboth, R. Fajardo Torres, N. Vachicouras, Q. Liu, N. Pavlova, S. Duis, A. Larmagnac, J. Vörös, S. Micera, Z. Suo, G. Courtine, S. P. Lacour, Electronic dura mater for long-term multimodal neural interfaces. *Science* **347**, 159–163 (2015).
4. D. Svirskis, J. Travas-Sejdic, A. Rodgers, S. Garg, Electrochemically controlled drug delivery based on intrinsically conducting polymers. *J. Control. Release* **146**, 6–15 (2010).
5. M. Sharma, G. I. N. Waterhouse, S. W. C. Loader, S. Garg, D. Svirskis, High surface area polypyrrole scaffolds for tunable drug delivery. *Int. J. Pharm.* **443**, 163–168 (2013).
6. C. Boehler, M. Asplund, A detailed insight into drug delivery from PEDOT based on analytical methods: Effects and side effects. *J. Biomed. Mater. Res.* **103**, 1200–1207 (2014).
7. L. Alonso-Nanclares, J. Gonzalez-Soriano, J. R. Rodriguez, J. DeFelipe, Gender differences in human cortical synaptic density. *Proc. Natl. Acad. Sci. U.S.A.* **105**, 14615–14619 (2008).
8. C. S. Klein, G. D. Marsh, R. J. Petrella, C. L. Rice, Muscle fiber number in the biceps brachii muscle of young and old men. *Muscle Nerve* **28**, 62–68 (2003).
9. J. Isaksson, P. Kjäll, D. Nilsson, N. Robinson, M. Berggren, A. Richter-Dahlfors, Electronic control of Ca^{2+} signalling in neuronal cells using an organic electronic ion pump. *Nat. Mater.* **6**, 673–679 (2007).
10. K. Tybrandt, K. C. Larsson, S. Kurup, D. T. Simon, P. Kjäll, J. Isaksson, M. Sandberg, E. W. H. Jager, A. Richter-Dahlfors, M. Berggren, Translating electronic currents to precise acetylcholine-induced neuronal signaling using an organic electrophoretic delivery device. *Adv. Mater.* **21**, 4442–4446 (2009).
11. A. Williamson, J. Rivnay, L. Kergoat, A. Jonsson, S. Inal, I. Uguz, M. Ferro, A. Ivanov, T. A. Sjöström, D. T. Simon, M. Berggren, G. G. Malliaras, C. Bernard, Controlling epileptiform activity with organic electronic ion pumps. *Adv. Mater.* **27**, 3138–3144 (2015).
12. D. T. Simon, S. Kurup, K. C. Larsson, R. Hori, K. Tybrandt, M. Goiny, E. W. H. Jager, M. Berggren, B. Canlon, A. Richter-Dahlfors, Organic electronics for precise delivery of neurotransmitters to modulate mammalian sensory function. *Nat. Mater.* **8**, 742–746 (2009).
13. A. Jonsson, Z. Song, D. Nilsson, B. A. Meyerson, D. T. Simon, B. Linderoth, M. Berggren, Therapy using implanted organic bioelectronics. *Sci. Adv.* **1**, e1500039 (2015).
14. K. Tybrandt, R. Forchheimer, M. Berggren, Logic gates based on ion transistors. *Nat. Commun.* **3**, 871 (2012).
15. E. Stavrinidou, P. Leleux, H. Rajaona, D. Khodagholy, J. Rivnay, M. Lindau, S. Sanaur, G. G. Malliaras, Direct measurement of ion mobility in a conducting polymer. *Adv. Mater.* **25**, 4488–4493 (2013).
16. D. M. DeLongchamp, B. D. Vogt, C. M. Brooks, K. Kano, J. Obrzut, C. A. Richter, O. A. Kirillov, E. K. Lin, Influence of a water rinse on the structure and properties of poly(3,4-ethylene dioxythiophene):poly(styrene sulfonate) films. *Langmuir* **21**, 11480–11483 (2005).
17. A. Elschner, S. Kirchmeyer, W. Lövenich, U. Merker, K. Reuter, *PEDOT: Principles and Applications of an Intrinsically Conductive Polymer* (CRC Press, 2010).
18. J. Rivnay, S. Inal, B. A. Collins, M. Sessolo, E. Stavrinidou, X. Strakosas, C. Tassone, D. M. Delongchamp, G. G. Malliaras, Structural control of mixed ionic and electronic transport in conducting polymers. *Nat. Commun.* **7**, 11287 (2016).
19. E. O. Gabrielsson, K. Tybrandt, M. Berggren, Ion diode logics for pH control. *Lab Chip* **12**, 2507–2513 (2012).
20. E. O. Gabrielsson, P. Janson, K. Tybrandt, D. T. Simon, M. Berggren, A four-diode full-wave ionic current rectifier based on bipolar membranes: Overcoming the limit of electrode capacity. *Adv. Mater.* **26**, 5143–5147 (2014).
21. H. Strathmann, *Ion-Exchange Membrane Separation Processes* (Elsevier, 2004).
22. K. Kontturi, L. Murtomäki, J. A. Manzanares, *Ionic Transport Processes* (Oxford Univ. Press, 2008).
23. Y.-A. Song, R. Melik, A. N. Rabie, A. M. S. Ibrahim, D. Moses, A. Tan, J. Han, S. J. Lin, Electrochemical activation and inhibition of neuromuscular systems through modulation of ion concentrations with ion-selective membranes. *Nat. Mater.* **10**, 980–986 (2011).
24. M. Ali, P. Ramirez, S. Mafé, R. Neumann, W. Ensinger, A pH-tunable nanofluidic diode with a broad range of rectifying properties. *ACS Nano* **3**, 603–608 (2009).
25. A. J. Bard, L. R. Faulkner, *Electrochemical Methods: Fundamentals and Applications* (John Wiley & Sons, ed. 2, 2001).

Acknowledgments: We wish to thank E. Gabrielsson for assistance with fabrication and analysis, and design of the control software. **Funding:** This work was supported by the Knut and Alice Wallenberg Foundation (KAW Scholar, 2012.0302), the Swedish Research Council (Vetenskapsrådet, 621-2011-3517), the Swedish Innovation Office (VINNOVA, 2010-00507), and the Önnesjö Foundation. **Author contributions:** A.J. and T.A.S. fabricated and optimized devices, and performed all experiments and analysis. A.J., T.A.S., K.T., M.B., and D.T.S. conceived the project. K.T., M.B., and D.T.S. guided the development of the project. A.J., T.A.S., and D.T.S. wrote the manuscript. **Competing interests:** K.T., M.B., and D.T.S. are shareholders in the small, researcher-controlled intellectual property company OBOE IPR AB (oboeipr.com), which owns the patents related to this research. **Data and materials availability:** All data needed to evaluate the conclusions in the paper are present in the paper and/or the Supplementary Materials. Additional data related to this paper may be requested from the authors.

Submitted 13 June 2016
Accepted 29 September 2016
Published 2 November 2016
10.1126/sciadv.1601340

Citation: A. Jonsson, T. A. Sjöström, K. Tybrandt, M. Berggren, D. T. Simon, Chemical delivery array with millisecond neurotransmitter release. *Sci. Adv.* **2**, e1601340 (2016).

Science Advances

Chemical delivery array with millisecond neurotransmitter release

Amanda Jonsson, Theresia Arbring Sjöström, Klas Tybrandt, Magnus Berggren and Daniel T. Simon

Sci Adv **2** (11), e1601340.
DOI: 10.1126/sciadv.1601340